Nuclear Instruments and Methods in Physics Research A 633 (2011) S282–S285

Contents lists available at ScienceDirect

Nuclear Instruments and Methods in Physics Research A

journal homepage: www.elsevier.com/locate/nima

Investigation of the potential use of $LaBr_3$:Ce scintillators for scintimammography imaging

Khalid S. Alzimami [a,b,*], Salem A. Sassi [c], Abdulrahman A. Alfuraih [a], Nicholas M. Spyrou [a,b]

[a] Department of Radiological Sciences, King Saud University, P.O. Box 10219, Riyadh 11432, Kingdom of Saudi Arabia
[b] Department of Physics, University of Surrey, Guildford, Surrey GU2 7XH, UK
[c] Joint Department of Physics, The Royal Marsden NHS Foundation Trust, Sutton, Surrey SM2 5PT, UK

ARTICLE INFO

Available online 19 June 2010

Keywords:
Scintimammography
$LaBr_3$:Ce
NaI(Tl)
GATE Monte Carlo simulation

ABSTRACT

The motivation of this study is to exploit the high light yield and excellent energy resolution of $LaBr_3$:Ce scintillators compared with NaI(Tl) crystal in scintimammograpic imaging systems. A dedicated gamma camera and 3D phantom were modelled using GATE Monte Carlo code under a variety of imaging situations including lession sizes, tumour activity-to-background ratios and tumour depths. The major finding of the present study is that $LaBr_3$:Ce crystal-based cameras have the potential to detect small lesions (≤ 10 mm) at clinical TBR.

1. Introduction

Being the most common and most feared malignancy in women, breast cancer is the second leading cause of cancer death in developed countries [1]. The gold standard of detecting breast cancer early is by screening mammography, which is currently the only screening method available that is proven to reduce breast cancer mortality [2]. However, this technique suffers from lower specificity and sensitivity and therefore patients with dense breasts have been admitted to undergo unnecessary biopsies [3].

Using standard gamma cameras in planar scintimammography has proven useful in the assessment of patients with breast lesions particularly in cases when mammography is imprecise and in women with dense breasts [4]. This technique, however, only demonstrates high sensitivity for tumours >1 cm in diameter [5] and therefore cannot be considered as a screening procedure. For this reason, great importance has been given to the development of dedicated cameras with high intrinsic spatial characteristics in order to enhance the sensitivity and specificity of small tumour detection with scintimammography. Use of a detector with a small field of view (FOV) allows greater flexibility in patient positioning, facilitating the acquisition of projections similar to those of X-ray mammography. Moreover, by placing the detector directly against the breast mild compression can also be applied to breast tissue, resulting in reduced breast thickness, increased target-to-background ratio and improved spatial resolution.

In addition to reducing breast (source) detector distance, the choice of detector material plays a vital role in improving breast lesion detectability. Cerium-doped lanthanum crystals, particularly $LaBr_3$:Ce, are of interest in SPECT imaging due to their high scintillation yield and superior energy resolution. When compared with NaI(Tl), $LaBr_3$:Ce has 60% more light output and better energy resolution (6–7% vs. 9% FWHM) [6]. LaBr3:Ce also has the added advantage of shorter attenuation length, which would reduce the scintillator volume by 25%, therefore improving intrinsic spatial resolution [7].

The main thrust of this study was to investigate the potential use of $LaBr_3$:Ce materials in the constuction of dedicated scintimammography gamma cameras in comparison with NaI(Tl), using GATE Monte Carlo simulations. Imaging performance was assessed by calculating signal-to-noise ratio (SNR) and simulated tumour full-width-half-maximum (FWHM) under a variety of imaging situations.

2. Monte Carlo simulations

Monte Carlo simulations are increasingly used in nuclear medicine imaging to assist in the design of new medical imaging devices for emission tomography. GEANT4 application for tomographic emission (GATE; version 3.1.2) as used in this study is a relatively new Monte Carlo simulation package based on GEANT4 dedicated to nuclear imaging applications [8]. GATE combines the advantages of the Geant4 simulation toolkit, well-validated physics models, complicated geometry description, powerful visualisation and time-dependent phenomena management. The GATE Monte Carlo simulation code has been extensively described and validated elsewhere [8–11].

* Corresponding author. Tel.: +966 1469 3567; fax: +966 1469 3565.
E-mail address: kalzimami@ksu.edu.sa (K.S. Alzimami).

0168-9002/$ - see front matter © 2010 Elsevier B.V. All rights reserved.
doi:10.1016/j.nima.2010.06.189

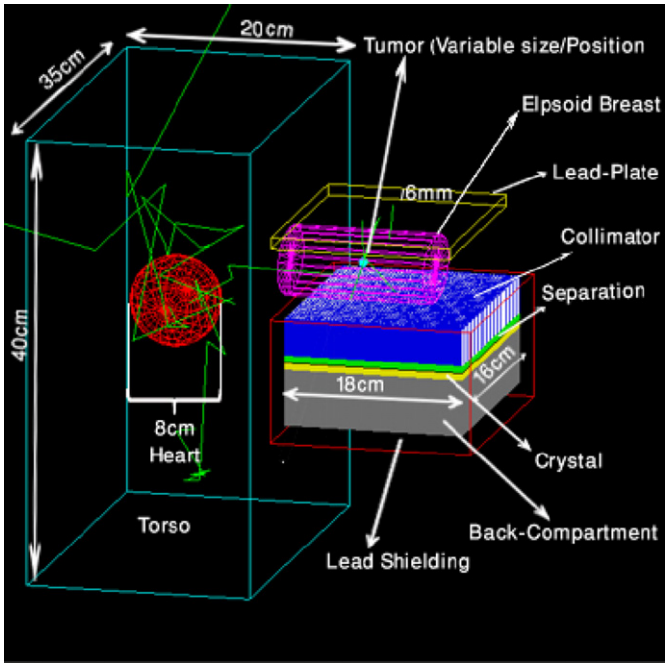

Fig. 1. A dedicated gamma camera and 3D phantom as modelled by GATE.

For this study, a single-head camera (Fig. 1) was modelled as a combination of:

- Low-energy high-resolution (LEHR) collimator made of lead (hole diameter: 1.22 mm, collimator thickness: 25.4 mm and septal thickness: 0.2 mm). Collimator holes are arranged in a hexagonal shape.
- Scintillator crystal ($180 \times 60 \times 6$ mm^{3}continuous $LaBr_3$:Ce or pixellated NaI(Tl); 2 mm pitch). Although, $LaBr_3$:Ce is commercially available in pixellated form, using continuous crystal does not limit the spatial resolution of the detector. Furthermore, energy resolution is worse in pixellated detector due to diminished light transmission.
- An aluminium sheet of 0.1 mm thickness was incorporated to simulate detector cover.
- A back-compartment was modelled as a 50 mm layer of Perspex (density 2.5 g/cm^3) to account for the photomultiplier tubes and electronics located behind the crystal.
- Shielding made of 8 mm thick lead around the camera head and 10 mm thick at the back.

The modelled phantom included:

- The upper body torso phantom was represented by a parallelepiped of $40 \times 35 \times 20$ cm^3.
- A spherical tumour (5 or 8 mm in diameter).
- An ellipsoid breast (length = 130 mm, height = 90 mm and width = 60 mm (semi-compressed)).
- A spherical heart (radius = 40 mm) and
- a lead plate with thickness of 6 mm was used to provide mild compression and to reduce the photon contamination from the upper torsos.

A background activity density of 3 kBq/cm^3 is assumed for the torso and breast phantom components, while the heart activity density is assumed to be 10 times greater based on Ref. [6]. Only 140 keV gamma rays from a $^{99}Tc^m$ isotropic source were simulated. Based on the phantom components' volume, the total number of simulated photons emitted was 6×10^{10} over a 10 min scan. Tumour activity-to-background ratio (TBR) concentration in the simulations is then varied ranging from 3:1 to 50:1. Tumor depth was varied from 10 or 40 mm.

Different materials (breast, heart and tissue), linked to their cross-sections for photon interaction, were specified in order to provide a realistic model phantom. The physics processes were modelled using the low energy electromagnetic processes package, including the Rayleigh, photoelectric and Compton interactions. A Gaussian energy blurring of FWHM = 15% and 6% at 140 keV, which follows $1/E^{-1/2}$ behaviour, and the intrinsic crystal resolution of 2.0 and 0.9 mm at 140 keV for NaI(Tl) and LaBr, respectively, were modelled based on Ref. [5]. A thresholder and upholder modules were used to apply 15% energy window centred on 140 keV. Simulations were run on a Linux cluster of five nodes, of which three were Sun Fire V20z (Processor 2.19 GHz with 8GB RAM) and two Sun Fire X4140 (Processor 2.3 GHz with 32GB RAM). The whole simulation process is controlled by the SUN grid engine.

3. Data analysis and results

As an example, Fig. 2 shows simulated planar scintimammographic images obtained from the LaBr3:Ce and NaI(Tl) crystal-based cameras under typical imaging conditions. It is difficult to compare these images qualitatively; therefore, images were assessed semi-quantitatively using SNR and tumour FWHM as the main criteria to compare the two simulated scintimmamography cameras.

All region-of-interest (ROI) analysis was performed using ROOT (V 5.12). Two ROIs were defined to calculate the SNR of the breast lesion. To ensure that all tumour events were included, a circular lesion (signal) ROI was defined as twice the FWHM of the system. Background ROI was defined over an area five times the FWHM of the system, excluding tumour area. The signal was defined as the difference between tumour and background ROI mean pixel values and the noise defined as the standard deviation in the background ROI.

Tumour spatial FWHM is of interest because it reveals how much the spatial resolution of the camera spreads out the lesion dimensions in the planar image. Values reported in this study were obtained by calculating the average of vertical, horizontal and diagonal profiles taken through the centre of the detected tumour in the simulated images after applying a Gaussian curve fit to the data.

Fig. 3 compares tumours FWHM values obtained from the $LaBr_3$:Ce and NaI(Tl) cameras at different imaging conditions; error bars on the plot represent the average of standard deviations of the Gaussian fit. Because of statistical variation in projection data and partial volume effects, obtained tumour FWHM values are smaller than the actual tumour size, particularly for lesion

Fig. 2. Exemplar of simulated planar scntimammographic images obtained from the $LaBr_3$:Ce (right) and NaI (left) crystal-based cameras under typical imaging conditions.

sizes below twice the FWHM of system's point spread function. Note that where appropriate Gaussian fits were not possible, FWHM results were not included. The improvement in the FWHM from the $LaBr_3$:Ce camera is due to the fact that $LaBr_3$:Ce has 60% higher light output than NaI(Tl). These improvements are of critical importance in the case of multiple gamma rays entring through the same hole of collimator. In addition, further resolution improvement could be achieved with the $LaBr_3$:Ce crystal by reducing crystal thickness with comparable sensitivity to the NaI(Tl) scintillator [12].

Fig. 4 shows the estimated tumour SNR values for 5 and 8 mm lesion at different TBRs. As expected, the SNR results are strongly dependent on the uptake ratios. On average, the $LaBr_3$:Ce camera improves SNR values by approximately 23% compared with those obtained with the NaI(Tl) crystal-based system. Note that SNR values obtained from the NaI(Tl) camera at TBR $\leq$ 20, for both tumour sizes (5 and 8 mm), are less than 10 nm suggesting poor lesion detectability. These SNR improvements are due to the higher system sensitivity of the $LaBr_3$:Ce crystals [12,13]. Furthermore, the superior energy resolution of the $LaBr_3$:Ce compared with the NaI(Tl) crystal could improve the primary to scatter ratio of detected counts and hence improve SNR. Fig. 5 shows comparable detected energy spectra for the same tumour ROI from the $LaBr_3$:Ce and NaI(Tl) crystal-based cameras under identical imaging conditions.

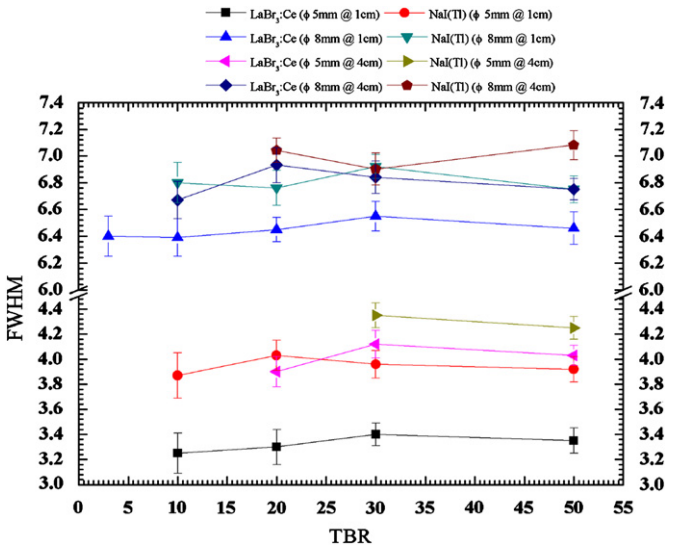

Fig. 3. Calculated tumour FWHM values as a function of TBR for 5 and 8 mm lesions at 10 and 40 mm depth.

4. Conclusions

In this preliminary study, we have semi-quantitatively compared imaging performance of the $LaBr_3$:Ce and NaI(Tl)

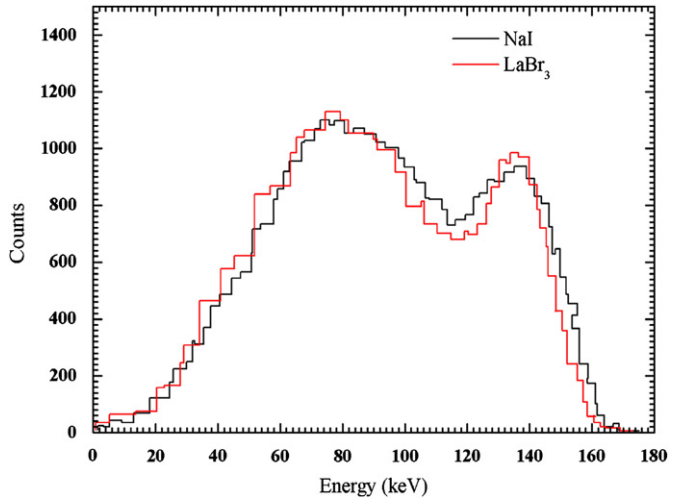

Fig. 5. Comparable detected energy spectra for the same tumour ROI from the $LaBr_3$:Ce and NaI(Tl) crystal-based cameras (TBR=10, 8 mm tumour, 10 mm depth).

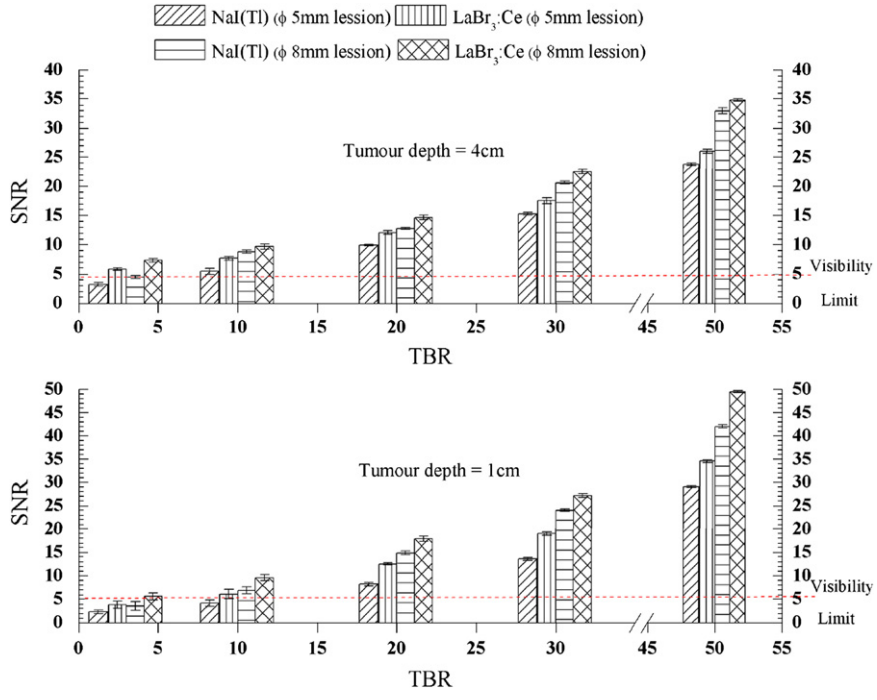

Fig. 4. Estimated tumour SNR values as a function of TBR for 5 and 8 mm lesions at 10 and 40 mm depth.

crystal-based dedicated scintimammography gamma cameras. The overall results suggest that the LaBr3:Ce crystals can further improve small breast lesions (≤ 10 mm) detectability with TBR ≥ 10 and have the potential to be the scintillator of choice for scintimammography. However, clinical investigations and low-cost crystal growth techniques are needed before $LaBr_3$:Ce scintillator be commonly used.

Acknowledgement

This study was supported by Medical Physics Research Group, King Saud University, Riyadh, Kingdom of Saudi Arabia.

References

[1] E.D. Pisano, et al., in: Digital Mammography, Lippincott Williams & Wilking, USA, 2004.
[2] Michael K. O'Connor, et al., Breast J. 13 (2007) 3.
[3] R. Pani, et al., Nucl. Instr. and Meth. A 497 (2003) 90.
[4] Orazio Schillaci, et al., J. Nucl. Med. 46 (2005) 550.
[5] R. Pani, et al., Nucl. Instr. and Meth. A 569 (2006) 296.
[6] R. Pani, et al., IEEE Trans. Nucl. Sci. NS-33 (1998) 3127.
[7] W.W. Mosesa, K.S. Shah, Nucl. Instr. and Meth. A 537 (2005) 317.
[8] S. Jan, et al., Phys. Med. Biol. 49 (2004) 4543.
[9] K. Assi, et al., Nucl. Instr. and Meth. A 527 (2004) 180.
[10] S. Staelens, et al., Phys. Med. Biol. 48 (2003) 3021.
[11] K Assie, et al., Phys. Med. Biol. 50 (2005) 3113.
[12] K. Alzimami, et al. in: Proceedings of the Fifth IEEE International Symposium on Biomedical Imaging Processing, Paris, 19–24 May 2008, p. 1243.
[13] R. Pani, et al., Nucl. Instr. and Meth. A 571 (2007) 475.